Published in final edited form as:
Biomech Model Mechanobiol. 2012 January ; 11(1-2): 171–182. doi:10.1007/s10237-011-0301-7.

Experimental measurement of dynamic fluid shear stress on the aortic surface of the aortic valve leaflet

Choon Hwai Yap, **Neelakantan Saikrishnan**, **Gowthami Tamilselvan**, and **Ajit P. Yoganathan**
Wallace H. Coulter School of Biomedical Engineering, Georgia Institute of Technology and Emory University, Room 2119 U. A. Whitaker Building, 313 Ferst Drive, Atlanta, GA 30332-0535, USA

Ajit P. Yoganathan: ajit.yoganathan@bme.gatech.edu

Abstract

Aortic valve (AV) calcification is a highly prevalent disease with serious impact on mortality and morbidity. Although exact causes and mechanisms of AV calcification are unclear, previous studies suggest that mechanical forces play a role. Since calcium deposits occur almost exclusively on the aortic surfaces of AV leaflets, it has been hypothesized that adverse patterns of fluid shear stress on the aortic surface of AV leaflets promote calcification. The current study characterizes AV leaflet aortic surface fluid shear stresses using Laser Doppler velocimetry and an in vitro pulsatile flow loop. The valve model used was a native porcine valve mounted on a suturing ring and preserved using 0.15% glutaraldehyde solution. This valve model was inserted in a mounting chamber with sinus geometries, which is made of clear acrylic to provide optical access for measurements. To understand the effects of hemodynamics on fluid shear stress, shear stress was measured across a range of conditions: varying stroke volumes at the same heart rate and varying heart rates at the same stroke volume. Systolic shear stress magnitude was found to be much higher than diastolic shear stress magnitude due to the stronger flow in the sinuses during systole, reaching up to 20 dyn/cm^2 at mid-systole. Upon increasing stroke volume, fluid shear stresses increased due to stronger sinus fluid motion. Upon increasing heart rate, fluid shear stresses decreased due to reduced systolic duration that restricted the formation of strong sinus flow. Significant changes in the shear stress waveform were observed at 90 beats/ min, most likely due to altered leaflet dynamics at this higher heart rate. Overall, this study represents the most well-resolved shear stress measurements to date across a range of conditions on the aortic side of the AV. The data presented can be used for further investigation to understand AV biological response to shear stresses.

Keywords

Native aortic valve; Aortic valve leaflet; Fluid shear stress; Laser Doppler velocimetry; Aortic surface; Heart valve fluid mechanics

1 Introduction

Calcific aortic valve disease is a highly prevalent disease affecting up to 2% of the elderly population (Lindroos et al. 1993); however, to date, the mechanism of the disease is unclear. Ex vivo studies suggest that mechanical forces such as pressure, membrane tension, and fluid shear stresses play an important role in mediating valve biology and pathobiology and could play a role in the development of this disease (Xing et al. 2004; Butcher et al. 2006;

Correspondence to: Ajit P. Yoganathan, ajit.yoganathan@bme.gatech.edu.

Balachandran et al. 2009; Sucosky et al. 2009; Smith et al. 2010). Fluid shear stress, in particular, was found to be protective against pro-inflammatory and pro-oxidative expressions in cultures of valvular endothelial cells (Butcher et al. 2006). Adverse patterns of shear stress were found to upregulate inflammatory markers in valve leaflet tissues (Sucosky et al. 2009). Further, it has been speculated that the reduced shear stresses on the non-coronary leaflet of the aortic valve (AV) due to the lack of coronary flow is responsible for the increased susceptibility to calcification of that leaflet (Freeman and Otto 2005).

In the arteries, it was found that vessels exposed to certain patterns of fluid shear stresses, such as low magnitude and oscillatory shear stress or "disturbed shear stress," are especially prone to atherosclerosis (Ku et al. 1985; Davies et al. 2005). Given the similarities in morphology between atherosclerosis and AV sclerosis lesions (Otto et al. 1994) and that these two diseases share common risk factors (Stewart et al. 1997; Agmon et al. 2001), one is inclined to hypothesize that similar mechanotransduction pathways of calcification may apply to AV leaflets as well. A complete understanding of the shear stress environment of the aortic valve leaflets is thus essential to understanding the pathways to aortic valve calcification. It has been hypothesized that the exposure of the two sides (aortic and ventricular surfaces) of the valve leaflet to different shear stress environments could be responsible for the preferential formation of calcification lesions on the aortic surface of the AV (Topper and Gimbrone 1999; Stevens et al. 2001; Weinberg et al. 2010). Thus, there is a need to characterize the shear stress environment on both surfaces. Further, it is well understood that the presence of mechanical forces is required for proper functioning of valve cells (Sarraf et al. 2002; Sacks et al. 2009), and thus, mechanical force conditioning is an essential step in tissue engineering of AVs. This step can only be performed appropriately with a good understanding of the native mechanical environment of the AV.

To this end, several authors have devoted efforts to simulating flow dynamics in the aortic valve, using fluid-structure interaction or computational fluid dynamics simulations (Makhijani et al. 1997; De Hart et al. 2003, 2004; Carmody et al. 2006; Morsi et al. 2007; Weinberg and Kaazempur Mofrad 2008; Ge and Sotiropoulos 2010; Weinberg et al. 2010). Collectively, these studies demonstrated the complex dynamics of flow and shear stress on the leaflets. However, the task of numerically modeling the aortic valve remains difficult. Complications exist in meshing the fluid–solid boundary, modeling the coupled fluid–solid interaction, modeling transitional flow and turbulence, and achieving Reynolds number of peak flow at physiological levels. Further, simulations require validation of modeling assumptions, and experimental measurements are the only reliable means of providing this validation.

Previously, only one study has attempted to experimentally measure fluid shear stresses on aortic valve leaflets. Weston et al. (1999) took Laser Doppler velocimetry (LDV) measurements on a tri-leaflet polymeric valve to obtain leaflet fluid shear stresses. However, only steady flow conditions were employed and the time-varying characteristics of shear stress were not shown. In addition, while non-invasive medical imaging modalities such as magnetic resonance imaging (MRI) and cardiac ultrasound seem to provide enticing means to evaluate the native fluid mechanical environment of the AV, these modalities have insufficient spatial and temporal resolution to do so. As such, experimental measurements of AV shear stresses must still be taken in vitro by employing physiological valve models using optical techniques.

In the current study, experimental measurements of time-varying shear stress on aortic valve leaflets were taken with LDV on an in vitro, fixed porcine AV as the valve model. High temporal resolution, two-dimensional shear stresses were measured on the ventricular surface of the valve leaflets. Shear stress measurements were taken over a range of

conditions of varying stroke volumes and heart rates to understand the effects of hemodynamics on shear stresses. The current study focuses only on aortic surface measurements and is one of the two manuscripts presenting fluid shear stresses on both surfaces of the AV.

2 Methods

2.1 Valve models

The valve model used in these studies is shown in Fig. 1. The valve had a diameter of 21 mm, a height of approximately 19 mm, and was constructed from a fresh porcine AV harvested from a local slaughterhouse. The valve was trimmed of its sinus walls, sutured to a plastic ring with three stents, and inserted into a clear acrylic aortic chamber with idealized tri-lobed sinuses designed to provide optical access for LDV work. The valve and chamber collectively constituted the valve model. The valve leaflets were colored black with tissue dye (Black Shandon® Tissue Marking Dye, Thermo-electron Corporation, Pittsburgh, PA) to reduce the reflection of LDV laser light off the leaflet surface. The acrylic aortic chamber was machined to have dimensions close to those noted earlier in rubber casts of human aortic root (Swanson and Clark 1974; Thubrikar 1990) in terms of the radial width of the sinuses and the axial heights, which were set to be 1.46 and 1.8 times the radius of the annulus. The valve chamber is shown in Fig. 1b.

2.2 Flow loop setup

The valve model was inserted into the Georgia Tech Left Heart Simulator, a pulsatile flow loop capable of mimicking left ventricular pressures and flow. Details of this loop can be found in previous publications (Leo et al. 2006; Yap et al. 2010), and a schematic is provided in Fig. 2. Thirty-six percentage glycerin solution was used as the working fluid to match the viscosity of blood (3.5 cSt). This fluid was selected because it was not damaging to native tissues. Due to the slight difference in refractive index between this solution and the acrylic chamber, optical distortion corrections were necessary. An ultrasonic flow probe (T108, Transonic System, Ithaca, NY) was placed directly upstream of the AV to measure trans-aortic volumetric flow rate, and pressure gauges (Baxter Uniflow pressure transducer, Baxter Healthcare corp., Irvine, CA), connected to the Cardiomed CM4008 (Medi-Stim, Oslo, Norway) were used to measure pressures directly upstream and downstream of the AV. Pressures and flow were recorded at 500 Hz with a data acquisition system (DAQ, National Instruments, Austin, TX) controlled by a custom-written Labview program.

The valve model was first tested under 70 beats/ min heart rate and 73-ml stroke volume, and shear stresses were characterized over the entire cardiac cycle to compare the differences between systolic and diastolic shear stresses. Following which, the valve was tested under two different sets of conditions and only systolic shear stresses were measured: (1) different stroke volumes (27, 43, 62, 68 ml) under the same heart rate (70 beats/ min) and (2) different heart rates (50, 70, 90 beats/ min) under the same stroke volume (55 ml). Aortic pressures were tuned to be 120/80 mmHg for all conditions. For experiments with varying heart rates, systolic durations were adjusted according to clinical data (Cui et al. 2008).

2.3 LDV Measurement technique

A fiber optic, three-component, coincident LDV system (Aerometric System, TSI Inc., Shoreview, MN) was used to measure velocities in the valve model. A 4-W Argon-ion laser was coupled to a fiber drive unit, allowing color separation of the incoming primary beam. A two-component fiber optic transceiver probe with a 100-mm focal length lens was connected to the fiber drive. The resulting optics train produced an ellipsoidal probe volume,

which, after accounting for the relative optical density between the flow loop fluid and air, had dimensions of 19 μm × 126 μm. Doppler signals were processed with Fast Fourier Transform based real-time signal analyzers (RSA-1000, TSI Inc., Shoreview, MN). All measurements were obtained in the backscatter mode in which a single probe acted as both the transmitter and receiver for the Doppler signals, and all measurements were gated to the pulse programmer, to phase lock the measurements to the cardiac cycle. The LDV system was set to a 5-MHz sampling frequency, giving a velocity resolution of 1.8 cm/s.

Velocities were measured at multiple points along a radial line between the sinus wall and the center of the valve, as shown in Fig. 3. Velocities were measured in the stream-wise direction only (from AV annulus to aorta), since this was the dominant component of the shear stress on the aortic surface. The distance between consecutive measurement points was 89 μm after correcting for changes in the refractive indices between the acrylic and the water glycerin solution. At least 40,000 data points were collected at each measurement location for statistical purposes, distributed over the entire cardiac cycle. At each location, velocity measurements were binned into 135–240 phases of 5 ms each over the entire cardiac cycle, according to the duration of the cardiac cycle.

2.4 Shear stress computation

In the computation of shear stress, the following assumptions were made: (1) Newtonian mechanics, specifically Galilean Invariance was valid and (2) the fluid was Newtonian and isotropic. The result of these assumptions was that shear stress was independent of the reference frame and could be defined as follows:

$$\tau_{ij}=\mu\left(\frac{\delta u_i}{\delta x_j}+\frac{\delta u_j}{\delta x_i}\right) \tag{1}$$

where μ is the dynamic viscosity of the fluid, u_i is the ith component of the velocity, and x_i is the position in the ith axis. The term in the parenthesis is collectively known as the shear rate. In this case, i is the streamwise direction and j is the radial direction. Thus, the first term of shear rate was obtained with the LDV-measured velocity profile by calculating the gradient of the streamwise velocity with respect to the radial distance, at the surface of the leaflet. The second term of shear rate was obtained by computing the relative radial velocity of adjacent points on the leaflet surface. An order of magnitude analysis was performed to show that the second term is small and is presented in the Appendix.

For all hemodynamic cases, shear stress was measured at the center of the valve leaflet, midway between the two commissures, and about 10 mm from the annulus of the valve. Velocities in the 15–20-measurement points nearest to the leaflet surface at the same time phase were used to calculate shear rate. These velocities were used to construct a periodic waveform by appending the data points with the negative mirror image of the same data points, using the location of the leaflet as the point of symmetry. A low-pass filter was then applied to the waveform to the 15th frequency mode, before the gradient of this velocity profile waveform was computed at the leaflet location. This method of interpolation was chosen so that no assumption on the shape of the flow profile would be needed.

To gauge the variability of shear stresses, the standard deviation of velocities at specific measurement locations at specific time bins was first calculated. These velocity standard deviations were then added to or subtracted from the ensemble mean velocities, to give the one standard deviation upper and lower bounds of velocities. The same shear stress calculation algorithms were then applied to these standard deviation bounds of velocities to yield the one standard deviation bounds of shear stress.

2.5 Leaflet location and orientation

To enable shear rate computation, the location of the leaflet surface must first be correctly identified. This was done by detecting the location where the back-scattered LDV laser light intensity recorded by the LDV probe was the highest, since the intensity of light reflected from the leaflet to the probe would be maximum when the leaflet is within the probe volume. Back-scattered laser light was received by the receiver fiber of the LDV probe and was sent to the photomultiplier box (PMT) through optical fiber cables. Raw signal output from the PMT was then recorded by the data acquisition system (DAQ, National Instruments, Austin, TX) at 500 Hz. At least 40 cardiac cycles of signals were recorded from the PMT and averaged to give ensemble-averaged back-scattered light intensity over 1 cardiac cycle. This averaging was done so that the randomly received Doppler Burst signals were eliminated, and only recurring high back-scattered light intensity, which was caused by the presence of leaflet, was recorded. At each time phase, intensity of back-scattered light was plotted over space and was reconstructed from its Fourier components to the 30th frequency mode, at a resulting spatial resolution of 200 points/mm, before the point of highest intensity was noted.

The orientation of the leaflet surface with respect to the LDV probe was important because velocity was measured in reference frame of the probe, while the goal of the current study is to obtain shear stress in the reference frame of the valve leaflets. In the current study, shear stress was first computed in the probe reference frame and later corrected to the orientation of the leaflet surface by the cosine of the angle between the leaflet and probe reference frame. To calculate this angle, leaflet location was measured at an additional point 0.64-mm downstream of the main measurement location. The leaflet orientation was calculated as the difference in leaflet location divided by distance between the two locations. This provided the angle necessary to this correction step.

3 Results

3.1 Experimental hemodynamics

Pressures across the valve simulated in the flow loop are shown in Fig. 4 for the physiological condition of 70 beats/ min heart rate and 62-ml stroke volume. The shapes of the pressure curves were similar for the other conditions. Due to its small size (21 mm), the valve was observed to have a maximum systolic pressure gradient of 16.3 mmHg, average systolic gradient of 10.1 mmHg, and an effective orifice area of approximately 1.22 cm^2. The systolic flow wave-forms for different stroke volumes at 70 beats/ min are shown in Fig. 5a, and for different heart rates at 55-ml stroke volume are shown in Fig. 5b. As expected, the volumetric flow rate increased with increasing stroke volume, and systolic duration decreased with increasing heart rate.

3.2 Leaflet dynamics

The reflected light intensity technique provided a description of the valve leaflet location along the scan line. Figure 6a shows the raw back-scattered light intensity map, demonstrating that the signals had little noise. Systolic positions of the leaflets are shown in Fig. 6b for the various stroke volume cases and Fig. 6c for the various heart rate cases. The systolic position of the valve leaflet was similar across all conditions, where the leaflet was opened further during early systole than late systole. Across different stroke volumes, systolic leaflet positions were less than 1 mm different from each other, and no obvious relationship between leaflet position and stroke volume was observed. At the lower stroke volumes, however, valve leaflets tended to close earlier due to slightly shorter systolic durations. At the higher heart rates, the valve leaflets started to move toward closure earlier, due to a decrease in systolic duration at higher heart rates. Systolic positions of the valve

leaflet were very similar for the 50 and the 70 beats/ min cases and were less than 0.1 mm apart. For the 90 beats/ min case, the valve leaflet was slightly further away from the sinus than the other two heart rate cases.

3.3 General shear stress characteristics

Fluid shear stress experienced by the leaflets at 70 beats/ min heart rate and 73-ml stroke volume is plotted over the entire cardiac cycle in Fig. 7, to demonstrate the general differences of shear stresses experienced during systole and diastole. Systolic shear stress was much higher in magnitude than in diastolic shear stresses. Systolic shear stress was observed to be similar to a half sine wave, but with delayed onset. Shear stresses were low during the first 1/3 of systole, rapidly increased to a peak approximately 21.3 dyn/cm^2 at mid-systole, and quickly decreased thereafter. Diastolic shear stress started at a lower peak of approximately 3.8 dyn/cm^2 during early diastole and gradually decreased to zero over the diastolic duration.

3.4 Shear stress across different stroke volume conditions

Since the initial measurements indicated that significant shear stress was observed only during systole, subsequent measurements focused on systolic shear stresses only. Figure 8 shows the fluid shear stress waveforms experienced during systole at the same point on the valve leaflet under different stroke volume conditions. The general characteristics of systolic shear stresses were preserved across different stroke volume conditions. Shear stresses were low during early systole and elevated during mid- to late systole. During early systole, immediately after valve opening, a low negative peak was observed in all the conditions. Thereafter, shear stresses were close to zero for the higher stroke volume cases and were slightly negative in the lower stroke volume cases. Shear stresses increased rapidly to the peak value at approximately the 275-ms time point and declined rapidly after that, getting close to zero at approximately the 350-ms time point. The measurements revealed that peak shear stress magnitude increased with increasing stroke volume. Late systolic peak shear stresses ranged from 1.1 dyn/cm^2 at 29-ml stroke volume to 15.0 dyn/cm^2 at 68-ml stroke volume, as displayed in Table 1a.

3.5 Shear stress across different heart rate conditions

Figure 8b shows the fluid shear stresses at the same point on the valve leaflet at different heart rates. At all heart rates, shear stresses were negative at early systole. Subsequently, the lower heart rates cases demonstrated the general characteristics such as low shear during early systole and the half sinusoid shear stress peak during late systole. At 90 beats/ min, however, the initial low shear stress characteristic was not observed, but was replaced by a rapid increase in shear stresses to the early systolic peak of approximately 5.4 dyn/cm^2. This was possibly due to the difference in valve leaflet dynamics at 90 beats/ min compared with the other two heart rates. Thereafter, shear stress decreased slightly before growing to the late systolic peak of approximately 7.8 dyn/cm^2. Between 50 and 70 beats/ min cases, slight differences were observed: the 70 beats/ min case had a lower late systolic peak shear stress of 10.2 dyn/cm^2, while the 50 beats/ min case had 11.4 dyn/cm^2. In the 50 beats/ min case, late systolic shear stress decline occurred later than in the 70 beats/ min case. As tabulated in Table 1b, the results showed that increased heart rate led to a reduction in the late systolic peak shear stress.

3.6 Variability of shear stresses

Figure 9 shows the one standard deviation bounds of measured shear stress for the various conditions investigated. Shear stresses appear to possess more variations during mid-to late systole. For cases with higher stroke volume and lower heart rate, shear stresses were more

variable during the flow deceleration phase and were low in variability during the flow acceleration phase. For cases with lower stroke volume and the case with the highest heart rate, shear stresses were more variable during mid-systole than during end-systole. With increasing stroke volume and decreasing heart rate, shear stress variability during mid-systole decreased.

4 Discussion

In the current study, general shear stress characteristics on the aortic surface of the valve leaflet as well as the effects of flow rate and heart rate on the shear stresses were measured.

The general shear stress characteristics described earlier can be explained by the interaction between sinus flow and valve leaflets. Sinus vortices are induced by the interaction between forward flow and fluid in the sinus volume. These vortices were first described by Bellhouse et al. (1969) using experimental data and theoretical modeling. It has also been studied in a number of in vitro investigations (Peskin and Wolfe 1978; Ming and Zhen-huang 1986) and more recently was measured in humans using phase contrast magnetic resonance imaging (Markl et al. 2005).

The interaction between the forward flow through the AV and fluid in the sinus can vary based on the opening angle of the valve. If the leaflet at peak systole opens into the sinus region, a portion of the forward jet directly enters the sinus, forming a sinus vortex due to the curvature of the sinus walls (Fig. 10b). In this case, there will be little delay between the peak flow and peak aortic shear stress. On the other hand, if the leaflet opening angle is smaller than 90°, the sinus vortex is formed due to entrainment of the quiescent sinus flow by the stronger forward jet, where the forward flow jet induces sinus flow by drag forces (Fig. 10a). This results in a larger delay in peak shear stresses after the peak flow. The shear stress measured in Fig. 7 most likely belonged to the latter, because shear stress elevation was delayed from the onset of systole. After peaking during late systole, shear stresses reduced due to viscous energy dissipation and the deceleration of forward flow, which reduced the intensity of the sinus vortex.

During late systole, flow reverses under adverse pressure gradient, resulting in fluid mixing. Subsequently, rapid closing motion of valve and fluid hammer on the valve causes further fluid mixing. These phenomena result in remnant fluid motion distal to the valve, which dissipates over the diastolic duration through viscous interactions. This can explain the characteristics of diastolic shear stress demonstrated in Fig. 7: a gradual decrease to zero. Nearing end diastole, however, ventricular contraction brought about reduction in transvalvular pressure, leading to minor motion of the valve before rapid valve opening, which led to small elevation of shear stresses. Diastolic shear stresses were observed to be small compared with systolic shear stresses.

In the current study, shear stress characteristics were observed to be a function of heart rate, stroke volume, and leaflet dynamics. Increased stroke volume was observed to increase systolic shear stresses. This was expected because a larger stroke volume will result in increased bulk forward flow rate, which would induce stronger sinus vortices, resulting in higher shear stresses. On the other hand, increased heart rate led to decrease in average systolic shear stress. This could be explained by the reduction in systolic duration with higher heart rate, resulting in insufficient time for high velocities to be induced in the sinus by bulk forward flow and consequently reduced shear stress on the valve leaflet. Increased heart rate at the same stroke volume implied that the early systolic bulk forward flow rates are higher, since the same amount of fluid must move through the valve within a shorter

period of time. This increase in forward flow rate was favorable to shear stress magnitude, but overall, shear stresses still reduced due to reduced systolic duration.

At 90 beats/ min, the valve leaflet was observed to have slightly different dynamics than the lower heart rates: the valve leaflet opened further during early systole (between 100 and 160 ms), but moved back toward the center thereafter (Fig. 6c). Further, bulk forward flow was higher than the other heart rates during early systole (between 100 and 220 ms) but lower in late systole. This initial wider leaflet opening and higher bulk forward flow rate during early systole were most likely the reason for early systolic elevation of positive shear stress compared with those observed in the other heart rate cases. The narrower leaflet opening and lower bulk forward flow rates during late systole (between 220- and 370-ms time points) were most likely the reason for late systolic reduction in shear stresses compared with those observed in the other heart rate cases. Immediately after leaflet opening, a small negative shear stress peak was observed for all the heart rate and flow rate conditions. This was mostly likely associated with the inertia of valve opening. At the 90 beats/ min condition, the valve leaflet was more dynamic during valve opening phase, so the initial negative shear stress peak was more prominent.

In terms of variability of shear stresses, higher variability was observed during mid- to late systole. This was likely because of the flow instabilities associated with increased velocities or that caused by the adverse pressure gradient in the valve. Adverse pressure gradient acted to decelerate forward flow during end-systole and could result in excessive mixing of fluid in the valve, which could result in instabilities. Increasing stroke volume appeared to reduce variability of shear stresses, which could be due to the development of more stable sinus vortex flows. Increasing heart rate, on the other hand, appeared to increase variability of shear stresses, which could be because of instabilities associated with more rapid fluid accelerations and higher leaflet dynamics.

The shear stress environment of the AV is poorly characterized to date, even though multiple studies investigating shear stress mechanobiology of the AV depend on it. In the absence of dynamic fluid shear stress data, investigators resorted to idealized shear stress waveforms for mechanobiology experiments, such as steady shear and sine waves (Butcher et al. 2004, 2006; Platt et al. 2006; Sucosky et al. 2009). The results from the current study showed that, contrary to past intuition (Butcher et al. 2008; Sucosky et al. 2009), shear stress on the aortic surface of the AV leaflet is mostly unidirectional, instead of oscillatory (constantly reversing in direction). Strong unidirectional shear stress was observed during systole due to the formation of sinus vortices. While this vortex can evolve to have a significant non-streamwise component, it is unlikely that the vortex will completely reverse in direction to render shear stress oscillatory. Further, shear stresses during diastole should be generally low since late systolic adverse pressure causes fluid mixing downstream of the valve and thus prevent formation of strong flow structures. Thus, while it is possible that before and after the sinus vortex formation, shear stresses can reverse to small negative values, it is unlikely that aortic shear stresses will look like a sine wave.

The varying hemodynamic conditions tested in the current study elucidated that aortic surface shear stress is strongly influenced by hemodynamic parameters. This indicates that any disease conditions with altered hemodynamics have the potential of affecting aortic surface shear stresses. It is currently unknown how alterations of shear stresses from its normal state will affect the AV biology. However, it is widely accepted that low and oscillatory shear stresses will lead to vascular endothelium sclerosis (Ku et al. 1985; Chatzizisis et al. 2007). If we assume a similar reaction of AV endothelium to shear stress as vascular endothelium, we can conclude that higher heart rates will reduce shear stress magnitude and potentially elicit sclerotic responses from the AV and that higher flow rate

will increase shear stress magnitudes, potentially reducing sclerotic responses from the AV. This notion corroborates with epidemiological findings that tachycardia is associated with increased risk of heart diseases (Kannel et al. 1987; Palatini 1999) and findings that tachycardia is associated with hypertension (Levy et al. 1946; Palatini et al. 1997), which is associated with increased risk of AV calcification (Pate 2002; Rabkin 2005). It further corroborates with research findings that exercise can prevent the formation of AV calcification (Matsumoto et al. 2010).

5 Limitations

The key limitation of this paper is the in vitro nature of the study with valve models. Consequently, it suffers from the limitations of any in vitro model—it cannot replicate exact in vivo conditions, such as pressure and flow waveforms, compliance of the native aortic root, and person-specific AV and aortic root geometry. Secondly, the preservation of the valve, which was done so that experiments could be carried out over extended period of time, resulted in changes in material properties of the valve (Vesely and Boughner 1989; Billiar and Sacks 2000), which might have altered leaflet dynamics to be closer to those of bioprosthetic valve rather than fresh AVs. Thirdly, the lack of coronary modeling in the current study rendered the diastolic shear stress results more applicable to the non-coronary leaflet than to the left or right coronary leaflets. We note, however, that the diastolic coronary flow has a low average velocity of 25 cm/s (Saito et al. 2008) and total flow per cycle of about 10% of the volume of a sinus and thus may not have very strong influence on diastolic sinus flow. Fourthly, although the sinus chamber was machined to match the radial width and axial height of human aortic sinuses as measured by previous investigators, the shape of the sinus may have differences with that of human aortic sinuses. In the sinus chamber, the sinuses took the shape of regular elongated sphere, while that of a human aortic sinus may be rounder and skewed toward the annulus. This difference in shape may lead to differences in the sinus vortex flow, which may lead to differences in shear stresses. Finally, the LDV technique was unable to obtain shear stress measurements during the time periods when valve leaflets were rapidly opening or closing. A more advanced surface mounted measurement technique might be needed to achieve this.

6 Conclusions

The current study presents in vitro measurements of shear stresses on the aortic surface of the AV leaflet. Systolic shear stress was shown to have higher magnitudes than diastolic shear stress. Systolic shear stresses were low during early systole but had a half sinusoid shape during late systole. Systolic shear stresses increased with higher stroke volume, decreased with higher heart rate, and increased with wider valve leaflet opening.

Acknowledgments

The authors would like to thank Holifield Farms for providing porcine heart samples for the experiments. Funding support from this work comes from the National Heart, Lung and Blood Institute grant number HL-07262 and from Tom and Shirley Gurley.

Appendix

This appendix will demonstrate that the second term in Eq. 1 is small compared with the first term, and thus analysis of shear stresses in the current study need only consider the first term. To make this comparison, we calculate the average of the absolute magnitude of term 1 (λ_1) and term 2 (λ_2) over systole:

$$\lambda_1 = \overline{|\text{Term1}|_{\text{systole}}} = \overline{\left|\frac{\delta u_i}{\delta x_j}\right|_{\text{systole}}} \quad (2)$$

$$\lambda_2 = \overline{|\text{Term2}|_{\text{systole}}} = \overline{\left|\frac{\delta u_j}{\delta x_i}\right|_{\text{systole}}} \quad (3)$$

Table 2 shows the values of λ_1 and λ_2 for the various hemodynamic conditions investigated in the current study. The results show that for all conditions except for the 29-ml stroke volume case, the second term was small, constituting less than 3.1% of the first term or less. For 29 ml case, this was 8.9%. The 1st term is determined by the fluid velocities in the sinus, while the second term is determined by the dynamics of the valve leaflet. In the 29 ml case, since fluid velocities were low, first term was smaller in magnitude, and the ratio of second term to first term was higher. Nonetheless, in all cases, the second term was at least 1 order of magnitude smaller than the first term and can be neglected with caution. In the current study, the first term is measured with much higher resolution than the second term, and thus, it is advantageous to neglect the second term.

The second term, however, is not universally negligible: the 29-ml stroke volume case demonstrated the possibility that the second term can become more dominant. Thus, the relative magnitude of the first and second term must always be checked for any simulations or experimental measurements for leaflet surface shear stresses.

References

Agmon Y, Khandheria BK, Meissner I, Sicks JR, O'Fallon WM, Wiebers DO, Whisnant JP, Seward JB, Tajik AJ. Aortic valve sclerosis and aortic atherosclerosis: different manifestations of the same disease? Insights from a population-based study. J Am Coll Cardiol. 2001; 38(3):827–834. [PubMed: 11527641]

Balachandran K, Sucosky P, Jo H, Yoganathan AP. Elevated cyclic stretch alters matrix remodeling in aortic valve cusps: implications for degenerative aortic valve disease. Am J Physiol Heart Circ Physiol. 2009; 296(3):H756–H764. [PubMed: 19151254]

Bellhouse BJ, Reid KG. Fluid mechanics of the aortic valve. Br Heart J. 1969; 31(3):391.

Billiar KL, Sacks MS. Biaxial mechanical properties of the natural and glutaraldehyde treated aortic valve cusp—Part I: experimental results. J Biomech Eng. 2000; 122(1):23–30. [PubMed: 10790826]

Butcher JT, Penrod AM, Garcia AJ, Nerem RM. Unique morphology and focal adhesion development of valvular endothelial cells in static and fluid flow environments. Arterioscler Thromb Vasc Biol. 2004; 24(8):1429–1434. [PubMed: 15117733]

Butcher JT, Simmons CA, Warnock JN. Mechanobiology of the aortic heart valve. J Heart Valve Dis. 2008; 17(1):62–73. [PubMed: 18365571]

Butcher JT, Tressel S, Johnson T, Turner D, Sorescu G, Jo H, Nerem RM. Transcriptional profiles of valvular and vascular endothelial cells reveal phenotypic differences: influence of shear stress. Arterioscler Thromb Vasc Biol. 2006; 26(1):69–77. [PubMed: 16293796]

Carmody CJ, Burriesci G, Howard IC, Patterson EA. An approach to the simulation of fluid-structure interaction in the aortic valve. J Biomech. 2006; 39(1):158–169. [PubMed: 16271600]

Chatzizisis YS, Coskun AU, Jonas M, Edelman ER, Feldman CL, Stone PH. Role of endothelial shear stress in the natural history of coronary atherosclerosis and vascular remodeling: molecular, cellular, and vascular behavior. J Am Coll Cardiol. 2007; 49(25):2379–2393. [PubMed: 17599600]

Cui W, Roberson DA, Chen Z, Madronero LF, Cuneo BF. Systolic and diastolic time intervals measured from Doppler tissue imaging: normal values and Z-score tables, and effects of age, heart rate, and body surface area. J Am Soc Echocardiogr. 2008; 21(4):361–370. [PubMed: 17628402]

Davies PF, Spaan JA, Krams R. Shear stress biology of the endothelium. Ann Biomed Eng. 2005; 33(12):1714–1718. [PubMed: 16389518]

De Hart J, Peters GW, Schreurs PJ, Baaijens FP. A three-dimensional computational analysis of fluid-structure interaction in the aortic valve. J Biomech. 2003; 36(1):103–112. [PubMed: 12485644]

De Hart J, Peters GW, Schreurs PJ, Baaijens FP. Collagen fibers reduce stresses and stabilize motion of aortic valve leaflets during systole. J Biomech. 2004; 37(3):303–311. [PubMed: 14757449]

Freeman RV, Otto CM. Spectrum of calcific aortic valve disease: pathogenesis, disease progression, and treatment strategies. Circulation. 2005; 111(24):3316–3326. [PubMed: 15967862]

Ge L, Sotiropoulos F. Direction and magnitude of blood flow shear stresses on the leaflets of aortic valves: is there a link with valve calcification? J Biomech Eng. 2010; 132(1) 014505.

Kannel WB, Kannel C, Paffenbarger RS Jr, Cupples LA. Heart rate and cardiovascular mortality: the Framingham study. Am Heart J. 1987; 113(6):1489–1494. [PubMed: 3591616]

Ku DN, Giddens DP, Zarins CK, Glagov S. Pulsatile flow and atherosclerosis in the human carotid bifurcation. Positive correlation between plaque location and low oscillating shear stress. Arteriosclerosis. 1985; 5(3):293–302. [PubMed: 3994585]

Leo HL, Dasi LP, Carberry J, Simon HA, Yoganathan AP. Fluid dynamic assessment of three polymeric heart valves using particle image velocimetry. Ann Biomed Eng. 2006; 34(6):936–952. [PubMed: 16783650]

Levy RL, White PD, et al. Transient tachycardia; prognostic significance alone and in association with transient hypertension. Med Press Egypt. 1946; 38(6):207–212. [PubMed: 20278752]

Lindroos M, Kupari M, Heikkila J, Tilvis R. Prevalence of aortic valve abnormalities in the elderly: an echocardiographic study of a random population sample. J Am Coll Cardiol. 1993; 21(5):1220–1225. [PubMed: 8459080]

Makhijani VB, Yang HQ, Dionne PJ, Thubrikar MJ. Three-dimensional coupled fluid-structure simulation of pericardial bioprosthetic aortic valve function. ASAIO J. 1997; 43(5):M387–M392. [PubMed: 9360067]

Markl M, Draney MT, Miller DC, Levin JM, Williamson EE, Pelc NJ, Liang DH, Herfkens RJ. Time-resolved three-dimensional magnetic resonance velocity mapping of aortic flow in healthy volunteers and patients after valve-sparing aortic root replacement. J Thoracic Cardiovasc Surg. 2005; 130(2):456–463.

Matsumoto Y, Adams V, Jacob S, Mangner N, Schuler G, Linke A. Regular exercise training prevents aortic valve disease in low-density lipoprotein-receptor-deficient mice. Circulation. 2010; 121(6): 759–767. [PubMed: 20124122]

Ming L, Zhen-huang K. Study of the closing mechanism of natural heart valves. Appl Math Mech. 1986; 7(10):955–964.

Morsi YS, Yang WW, Wong CS, Das S. Transient fluid-structure coupling for simulation of a trileaflet heart valve using weak coupling. J Artif Organs. 2007; 10(2):96–103. [PubMed: 17574512]

Otto CM, Kuusisto J, Reichenbach DD, Gown AM, O'Brien KD. Characterization of the early lesion of 'degenerative' valvular aortic stenosis. Histological and immunohistochemical studies. Circulation. 1994; 90(2):844–853. [PubMed: 7519131]

Palatini P. Elevated heart rate as a predictor of increased cardiovascular morbidity. J Hypertens Suppl. 1999; 17(3):S3–S10. [PubMed: 10489092]

Palatini P, Casiglia E, Pauletto P, Staessen J, Kaciroti N, Julius S. Relationship of tachycardia with high blood pressure and metabolic abnormalities: a study with mixture analysis in three populations. Hypertension. 1997; 30(5):1267–1273. [PubMed: 9369286]

Pate GE. Association between aortic stenosis and hypertension. J Heart Valve Dis. 2002; 11(5):612–614. [PubMed: 12358395]

Peskin CS, Wolfe AW. The aortic sinus vortex. Fed Proc. 1978; 37(14):2784–2792. [PubMed: 720632]

Platt MO, Xing Y, Jo H, Yoganathan AP. Cyclic pressure and shear stress regulate matrix metalloproteinases and cathepsin activity in porcine aortic valves. J Heart Valve Dis. 2006; 15(5): 622–629. [PubMed: 17044366]

Rabkin SW. The association of hypertension and aortic valve sclerosis. Blood Press. 2005; 14(5):264–272. [PubMed: 16257871]

Sacks MS, Schoen FJ, Mayer JE. Bioengineering challenges for heart valve tissue engineering. Annu Rev Biomed Eng. 2009; 11:289–313. [PubMed: 19413511]

Saito M, Okayama H, Nishimura K, Ogimoto A, Ohtsuka T, Inoue K, Hiasa G, Sumimoto T, Higaki J. Possible link between large artery stiffness and coronary flow velocity reserve. Heart. 2008; 94(6):e20. [PubMed: 17947361]

Sarraf CE, Harris AB, McCulloch AD, Eastwood M. Tissue engineering of biological cardiovascular system surrogates. Heart Lung Circ. 2002; 11(3):142–150. discussion 151. [PubMed: 16352087]

Smith KE, Metzler SA, Warnock JN. Cyclic strain inhibits acute pro-inflammatory gene expression in aortic valve interstitial cells. Biomech Model Mechanobiol. 2010; 9(1):117–125. [PubMed: 19636599]

Stevens T, Rosenberg R, Aird W, Quertermous T, Johnson FL, Garcia JG, Hebbel RP, Tuder RM, Garfinkel S. NHLBI workshop report: endothelial cell phenotypes in heart, lung, and blood diseases. Am J Physiol Cell Physiol. 2001; 281(5):C1422–C1433. [PubMed: 11600404]

Stewart BF, Siscovick D, Lind BK, Gardin JM, Gottdiener JS, Smith VE, Kitzman DW, Otto CM. Clinical factors associated with calcific aortic valve disease. Cardiovascular health study. J Am Coll Cardiol. 1997; 29(3):630–634. [PubMed: 9060903]

Sucosky P, Balachandran K, Elhammali A, Jo H, Yoganathan AP. Altered shear stress stimulates upregulation of endothelial VCAM-1 and ICAM-1 in a BMP-4- and TGF-beta1-dependent pathway. Arterioscler Thromb Vasc Biol. 2009; 29(2):254–260. [PubMed: 19023092]

Swanson M, Clark RE. Dimensions and geometric relationships of the human aortic valve as a function of pressure. Circ Res. 1974; 35(6):871–882. [PubMed: 4471354]

Thubrikar, M. The aortic valve. Florida: Boca Raton; 1990.

Topper JN, Gimbrone MA Jr. Blood flow and vascular gene expression: fluid shear stress as a modulator of endothelial phenotype. Mol Med Today. 1999; 5(1):40–46. [PubMed: 10088131]

Vesely I, Boughner D. Analysis of the bending behaviour of porcine xenograft leaflets and of natural aortic valve material: bending stiffness, neutral axis and shear measurements. J Biomech. 1989; 22(6–7):655–671. [PubMed: 2509479]

Weinberg EJ, Kaazempur Mofrad MR. A multiscale computational comparison of the bicuspid and tricuspid aortic valves in relation to calcific aortic stenosis. J Biomech. 2008; 41(16):3482–3487. [PubMed: 18996528]

Weinberg EJ, Mack PJ, Schoen FJ, Garcia-Cardena G, Kaazempur Mofrad MR. Hemodynamic environments from opposing sides of human aortic valve leaflets evoke distinct endothelial phenotypes in vitro. Cardiovasc Eng. 2010; 10(1):5–11. [PubMed: 20107896]

Weston MW, LaBorde DV, Yoganathan AP. Estimation of the shear stress on the surface of an aortic valve leaflet. Ann Biomed Eng. 1999; 27(4):572–579. [PubMed: 10468241]

Xing Y, Warnock JN, He Z, Hilbert SL, Yoganathan AP. Cyclic pressure affects the biological properties of porcine aortic valve leaflets in a magnitude and frequency dependent manner. Ann Biomed Eng. 2004; 32(11):1461–1470. [PubMed: 15636107]

Yap CH, Dasi LP, Yoganathan AP. Dynamic hemodynamic energy loss in normal and stenosed aortic valves. J Biomech Eng. 2010; 132(2) 021005.

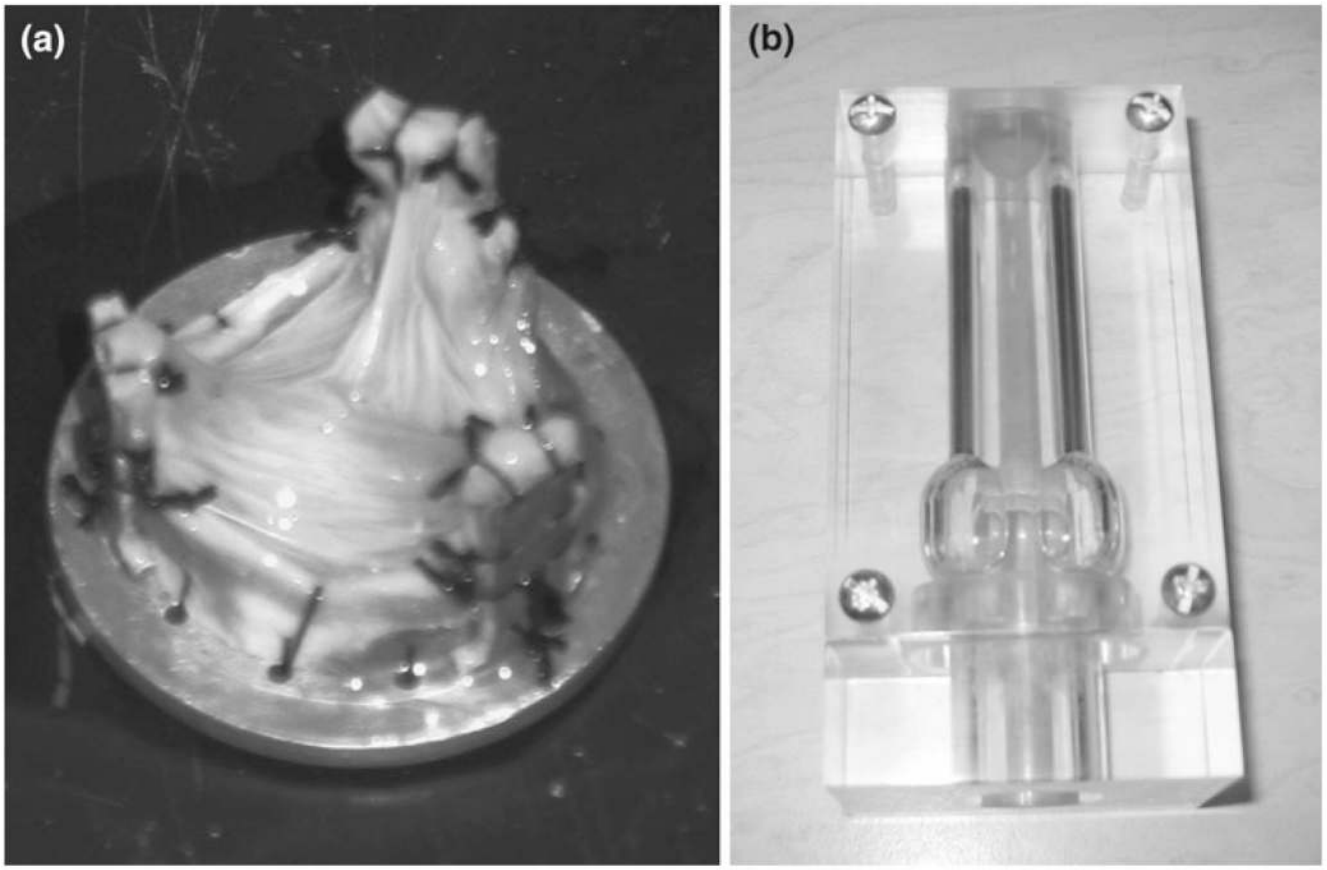

Fig. 1.
Native valve models used for the study: **(a)** fresh porcine valve trimmed and sutured onto a plastic ring with three stents, and fixed in 0.2% glutaraldehyde solution; **(b)** the acrylic chamber with three-lobed idealized sinus geometry used to house the valve

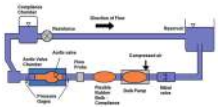

Fig. 2.
Schematic of the pulsatile flow loop used to expose the valve model to various hemodynamic conditions. The loop is driven by compressed air pressing on a bulb pump located between the subject aortic valve and a mechanical mitral valve. Bulk forward flow rate and pressures upstream and downstream of the aortic valve were measured

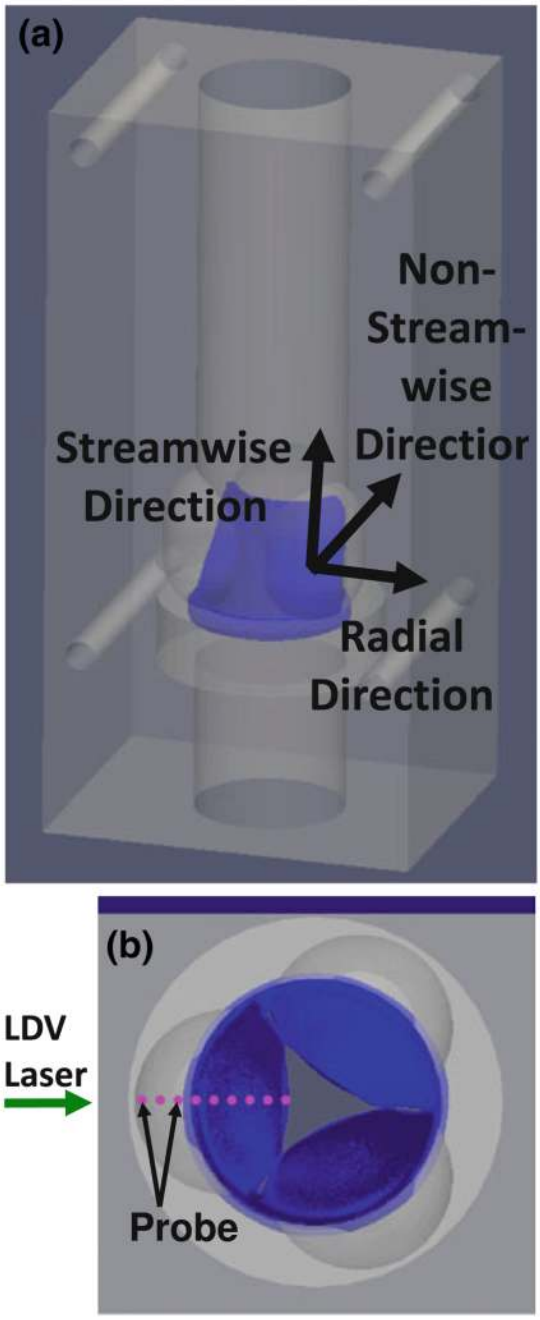

Fig. 3.

(a) Definition of directions of velocity and shear stress measurements. The streamwise direction is defined as the direction pointing downstream, while the non-streamwise direction is defined as the direction from one commissure to the next. **(b)** Schematic of LDV velocity measurement scheme. Velocities in were measured at intervals of 89 microns along a straight line at the center of the valve leaflet

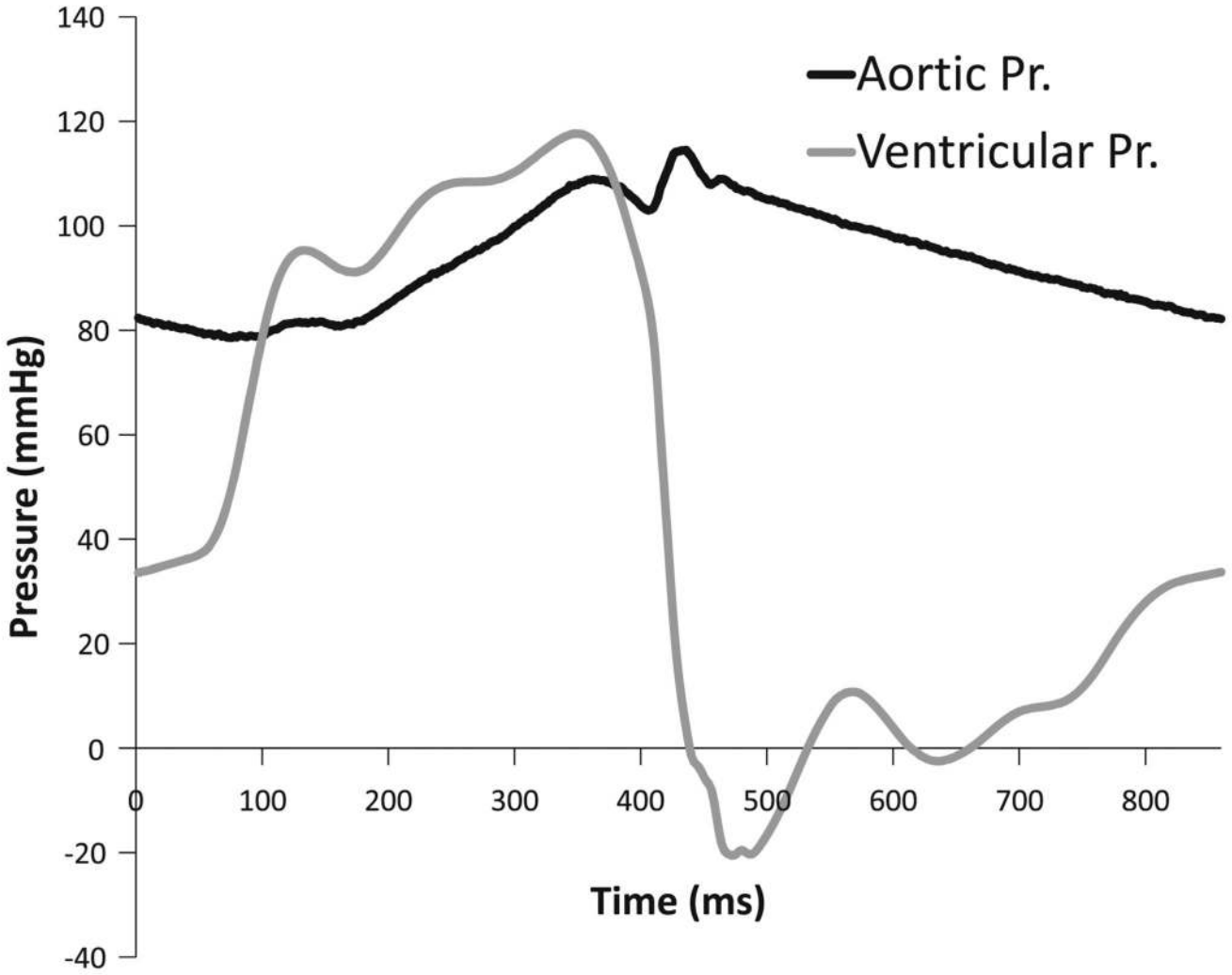

Fig. 4.
Typical pressure waveform simulated for the valve model. Aortic pressure is controlled to be between 80 mmHg and 120 mmHg

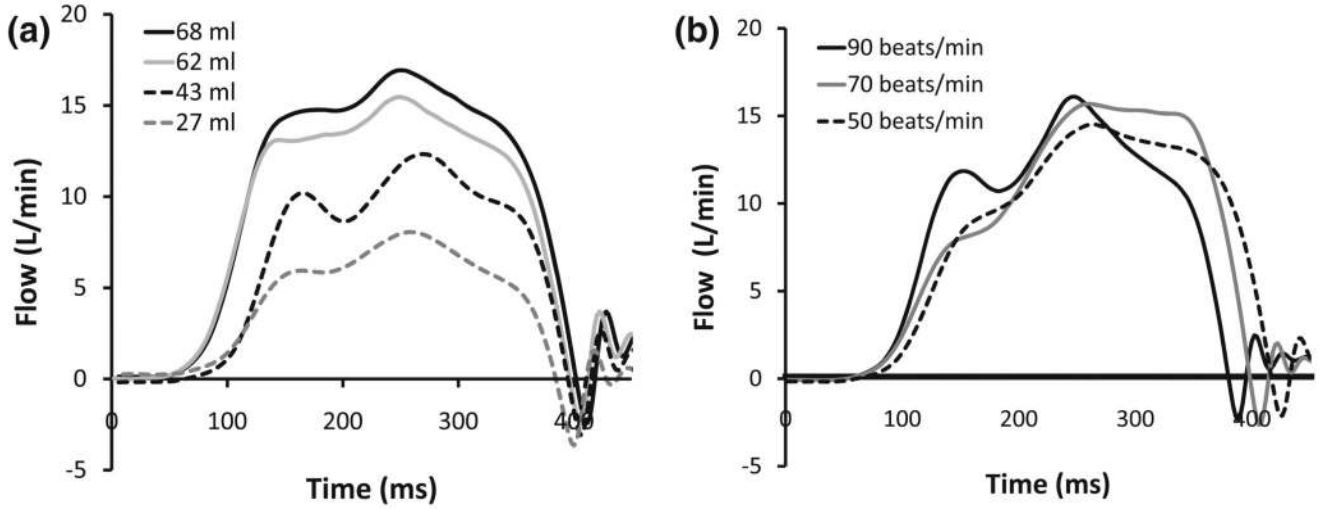

Fig. 5.

(a) Flow waveforms over systole for different stroke volume conditions at the same heart rate of 70 beats/ min; and **(b)** flow waveforms over systole for different heart rate conditions at the same stroke volume of 55 ml

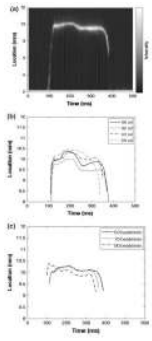

Fig. 6.

(a) Representative back-scattered light intensity map: ensemble-averaged back-scattered light intensity along the line of measurement over time, showing the trajectory of the valve leaflet during systole. The leaflet opened at 100-ms time point and closed at 400-ms time point. **(b)** Valve leaflet position during systole for the various stroke volume conditions at the same heart rate of 120 beats/ min; and **(c)** valve leaflet position for different heart rate conditions at the same stroke volume of 55ml, obtained by segmenting the back-scattered light intensity map

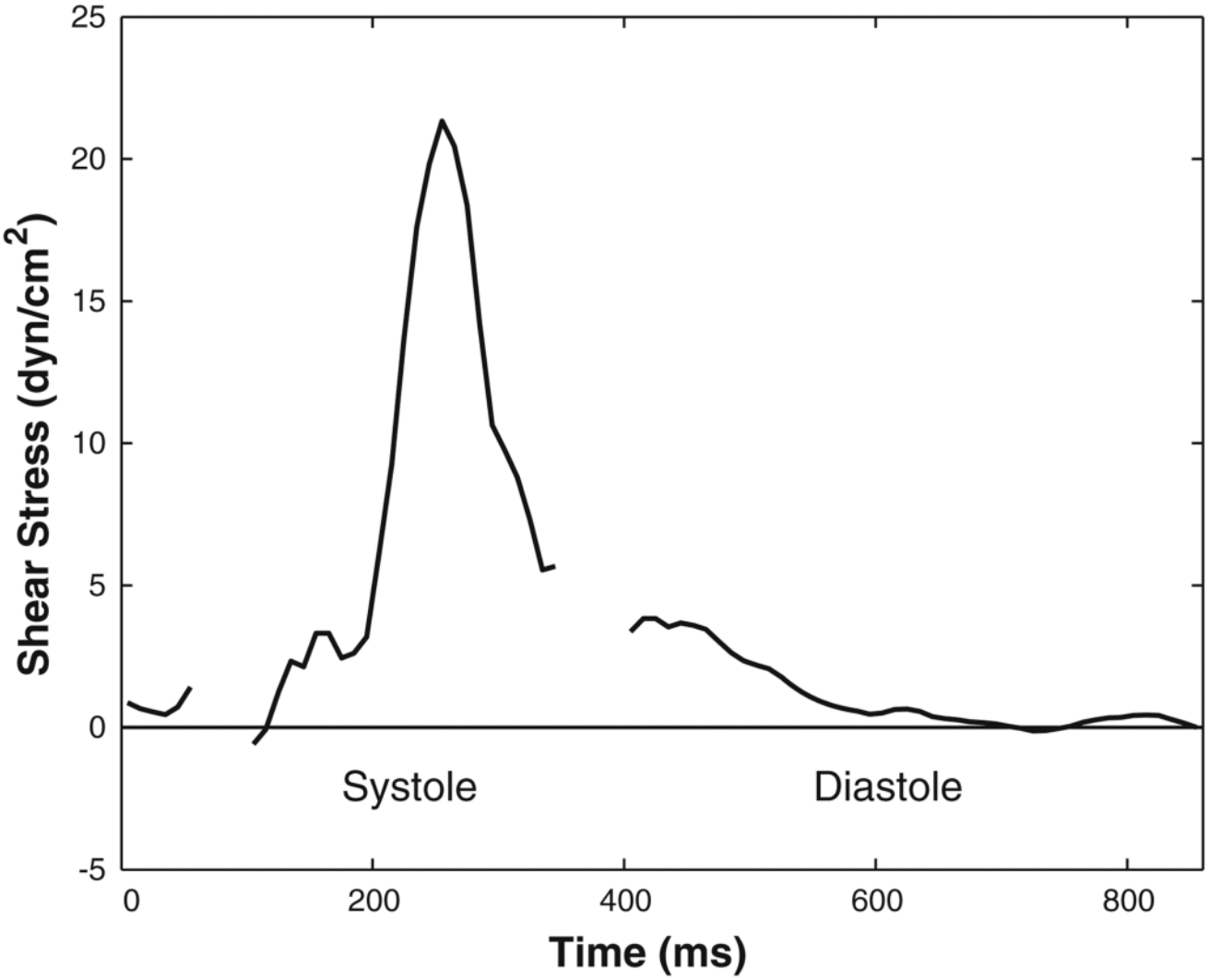

Fig. 7.
Shear stresses experienced by the aortic valve over the cardiac cycle, demonstrating that systolic shear stresses were higher in magnitude than diastolic shear stresses

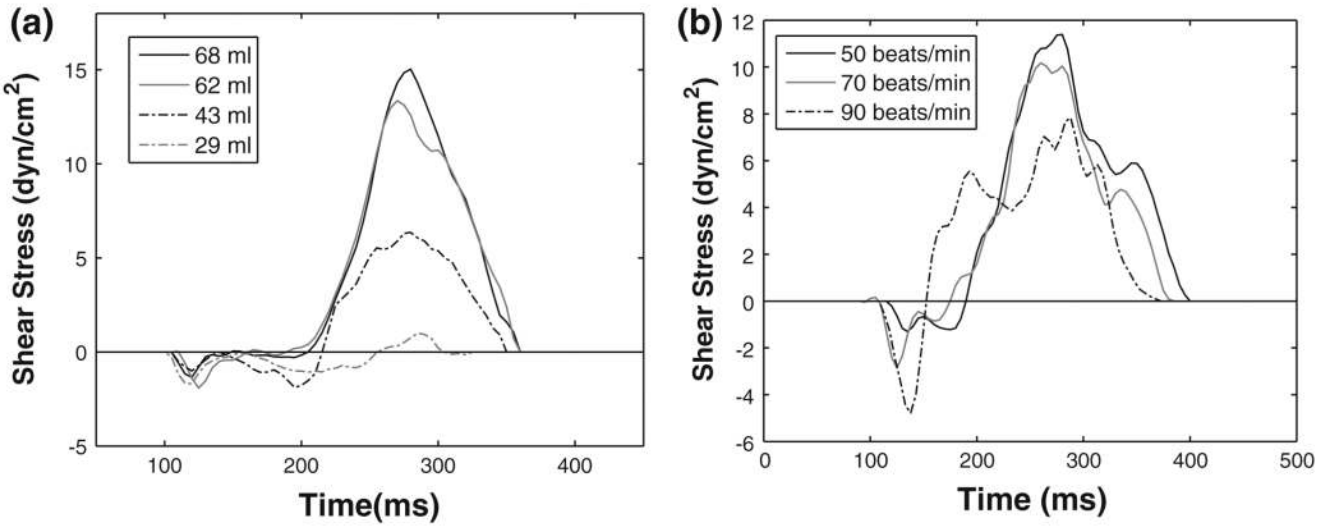

Fig. 8.

Shear stress waveforms over systole for **(a)** different stroke volume conditions at the same heart rate of 120 beats/ min; and **(b)** different heart rate conditions at the same stroke volume of 55 ml

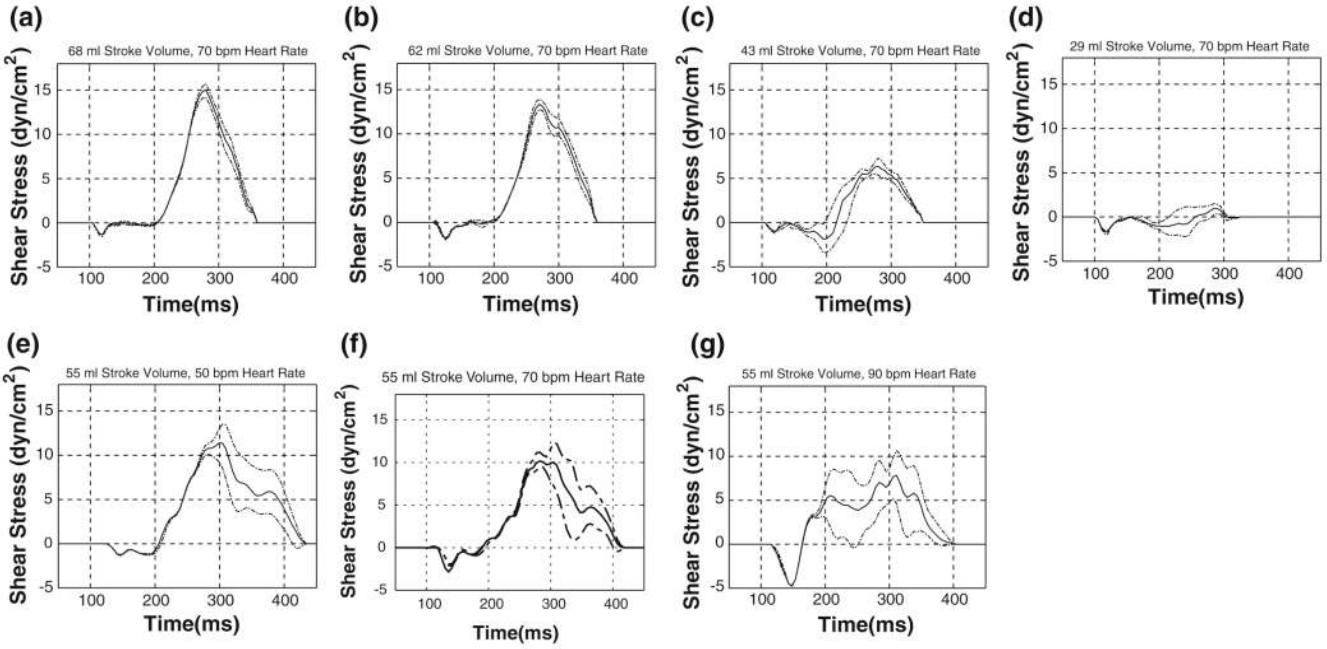

Fig. 9.

Measured shear stresses at various stroke volume and heart rate conditions and the one standard deviation bounds of the measured shear stresses

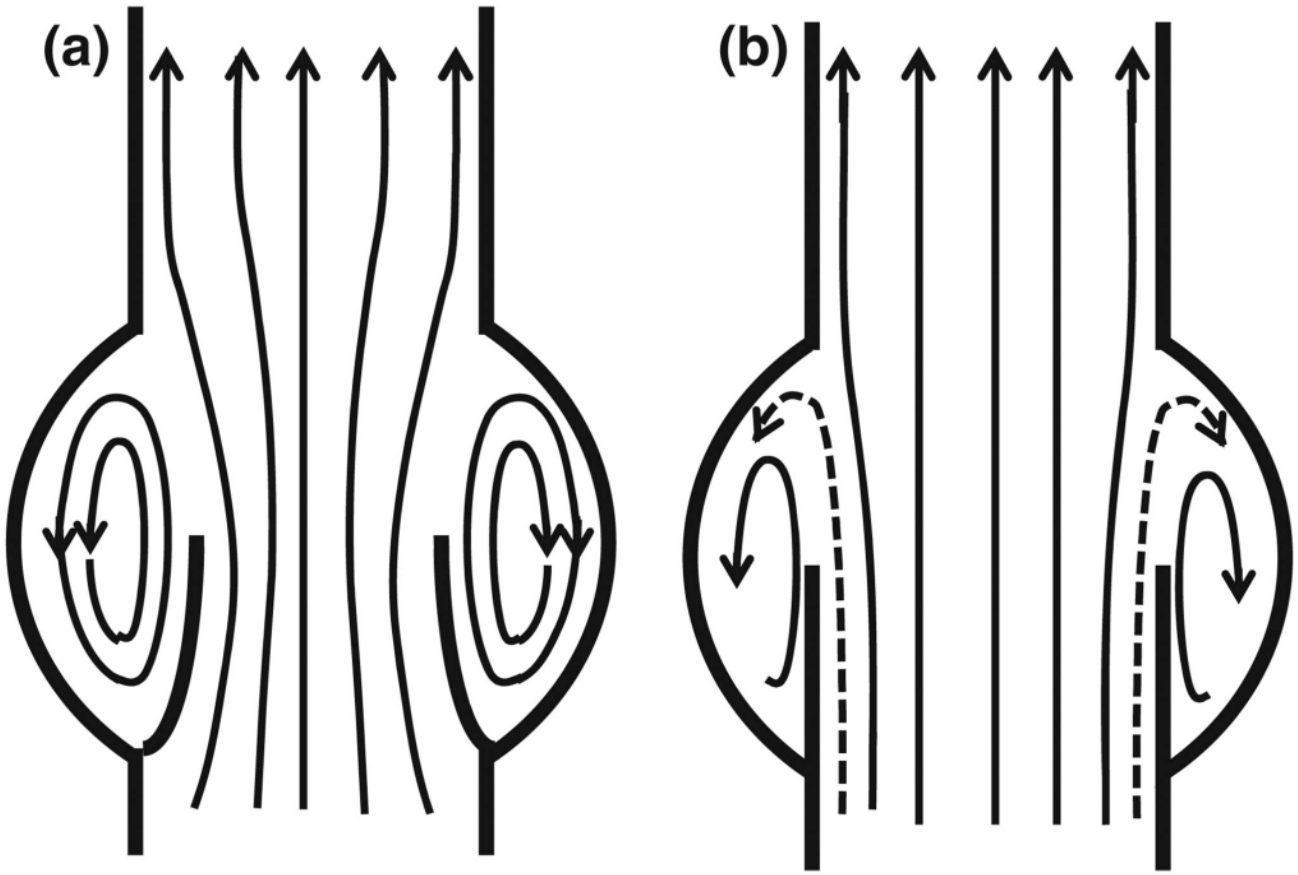

Fig. 10.
Schematic of possible mechanism of sinus vortex induction. **a** Sinus vortex is induced by shear forces of the adjacent forward flow jet. **b** Sinus vortex is induced by part of the forward flow entering the sinus after encountering the sinotubular junction

Table 1

Peak shear stresses for (a) the different stroke volume conditions at the same heart rate of 70 beats/ min, and (b) the different heart rate conditions at the same stroke volume (55ml)

Heart rate (beats/ min)	Stroke volume (ml)	Peak shear stress (dyn/cm^2)
(a)		
70	68	15.0
70	62	13.4
70	43	6.4
70	29	1.1
(b)		
50	55	11.4
70	55	10.2
90	55	7.8

Table 2

Order of magnitude comparison of the 1st term of the shear rate (Eq. 1) compared the 2nd term

Stroke volume (ml)	68	62	43	29	55	55	55
Heart rate (bpm)	70	70	70	70	50	70	90
λ_1 (%)	1.17	1.27	0.85	0.15	1.29	1.06	1.04
λ_2 (%)	0.010	0.015	0.015	0.013	0.021	0.030	0.033
λ2/λ1 (%)	0.8	1.1	1.8	8.7	1.6	2.8	3.1

Maximum values of the 1st term and the 2nd term were compared in various stroke volume and heart rate cases investigated